Electrical Power and Energy Systems 155 (2024) 109685

Contents lists available at ScienceDirect

International Journal of Electrical Power and Energy Systems

journal homepage: www.elsevier.com/locate/ijepes

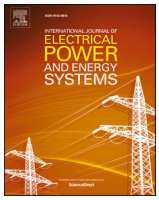

Modeling of power reactors for VFTO simulations: Full-scale design in a real application

André S. Melo [a], Eduardo C. Marques da Costa [a,*], Wilerson V. Calil [a], Ronaldo F. Ribeiro Pereira [b], Felipe P. de Albuquerque [a]

[a] Department of Electronic Systems Engineering, Polytechnic School – University of São Paulo POLI-USP, Brazil
[b] Federal University of Acre – UFAC, Rio Branco, Brazil

ARTICLE INFO

Keywords:
Power reactors
Finite element method
Very fast electromagnetic transients

ABSTRACT

The shunt reactors operate under a very specific conditions in Gas Insulated Substations - GIS, especially during very fast electromagnetic transients due to switching and maneuver operations. A meticulous electromagnetic analysis for correct design of such power devices, especially on the insulation coordination between turns, discs, and from winding to ground. This article presents a step-by-step modeling methodology based on the Finite Element Method, which is applied during the conception and manufacturing of a real shunt reactor for GISs. Finally, the time- and frequency-domain simulations are compared with experimental data obtained from laboratory tests.

1. Introduction

The rotate power machines, transformers and shunt reactors are usually represented by equivalent magnetic and electric circuits with gapped core and complex winding design, which are concepted to withstand standardized tests and operational demands. There are several computer-aided design CAD tools applied for modeling and simulation of electrical power machines in mechanical, thermal and electromagnetic terms. For example, electric rotating motors and power transformers are subjected to intense electromechanical transients, permanent mechanical vibration, thermal dissipation in the windings and core, stray losses due to magnetic leakage flux, dielectric stress on the electrical insulation, and several other destructive effects. In this context, meticulous and accurate modeling methodologies are required for proper design and manufacturing of electric power machines.

The internal windings of power transformers and shunt reactors are exposed to severe transient overvoltages during switching and maneuver operations. In this context, some models have been proposed for electromagnetic transient simulations, which are mostly based on the equivalent electric circuit approach and transmission line modeling. The internal capacitance and inductance of the winding are represented by lumped element circuits in such white-box models [1–3]. However, these models have a complex representation of the electromagnetic coupling by using equivalent circuit and matrix techniques [4].

Such power reactors could be modeled accurately in the frequency domain, with the equivalent two-port model and numerical transforms to determine the current and frequency transients in the time domain. Nevertheless, this frequency-domain approach shows several restrictions for representation of time-varying phenomena and components during simulations. Otherwise, the modeling directly in the time domain show to be versatile and reliable for transient simulations with time-varying elements [4].

In this context, the *Gas Insulation Substations* – GISs represent a relatively new technology in power systems applications. Several advantages raised from the electric insulation with the greenhouse gas *sulphur hexafluoride* SF_6, such as: significant improving in the insulating performance for interrupting arcs and size reducing of substations. This technology has been widely applied in power transmission systems and petrochemical plants [5,6]. However, the rapid arc interrupting results in very fast transient overvoltages – VFTOs in some parts of the substation circuits, which have led to most faults in GISs. These electromagnetic transients are composed of a wide range of frequencies and wave front in the time scale of nanoseconds [7].

The modeling of shunt reactor, for very fast transient simulations, still represents a challenge for industrial and research applications. The conventional models and circuit approaches are not well established, which leads to uncertainties during design and manufacture of such power equipment in SF_6 applications. In this sense, this paper proposes a

* Corresponding author.
E-mail address: educosta@usp.br (E.C. Marques da Costa).

https://doi.org/10.1016/j.ijepes.2023.109685
Received 20 April 2023; Received in revised form 3 October 2023; Accepted 24 November 2023
Available online 30 November 2023

complete modeling and simulation methodology based on the concept and manufacture of a full-scale reactor for a real GIS application.

Initially, the physical structure of the shunt reactor is described in terms of characterization of materials and geometric details. In sequence, the winding is modeled using a computer-aided design CAD platform based on the Finite Element Method – FEM for electromagnetic analysis. From such FEM-based analysis, the electrical parameters of the shunt reactor can be calculated, such as: inductance, series capacitance, capacitance between discs and other parallel capacitances [8,9]. Since the mechanical characteristics and electrical parameters are determined, the winding can be modeled and simulated by means of electrical circuits directly in the time domain.

All parameters and results simulated from the proposed modeling methodology are compared to experimental data obtained in experimental tests with a real full-scale reactor, which was designed to a GIS by a world-renowned manufacturer.

2. Shunt reactor structure and mechanical characteristics

A power shunt reactor of 30 MVAr is designed with 3000 turns in discs and nominal voltage 500 kV. Figs. 1 and 2 describe the main mechanical characteristics of the disc configuration in high-voltage windings [9,10].

Fig. 1 shows a single conductor around a central axis, which is defined as a *single turn*, whereas a radial set of coaxial turns is defined as *disc* or *coil* [9]. Fig. 2 describes the winding structure by overlapping discs, which is widely applied to design high-voltage transformers and shunt reactors [9,10]. The *inner* and *outer crossovers*, also defined as *S-bend*, form a secondary coaxial disc. The overlapping first and secondary discs compose a *double disc*, which is the elementary structure of the winding in the Fig. 2.

There are three principal types of disc windings: the ordinary disc winding (DO), interleaved disc (DI), shielded disc winding (DS), and combination of these three types. The shunt reactor in this work was designed based on ordinary and interleaved disc winding configurations, since the shielded discs are an extension of DO type [11]. The ordinary or continuous disc winding is characterized by just one disc, where the coaxial turns are placed side by side on the radial plane with only one turn voltage difference between parallel conductors. Fig. 3 illustrates the main features of the DI and DO configurations.

The shunt reactors are designed to store a certain amount of reactive power under a nominal voltage, normally such power is in the scale of MVAr. In this sense, an electric current should be established across the windings, which means that a gapped core is required to fit the inductance value of the shunt reactor to limit such current [11]. Another important issue is the clearance between the core and winding, which is directly to the line and ground terminals, and therefore subject to high electric gradients. Even the neutral terminal still requires enough dielectric distance to grounded parts, which are usually defined as standard levels of electric insulation in the technical literature [12–14].

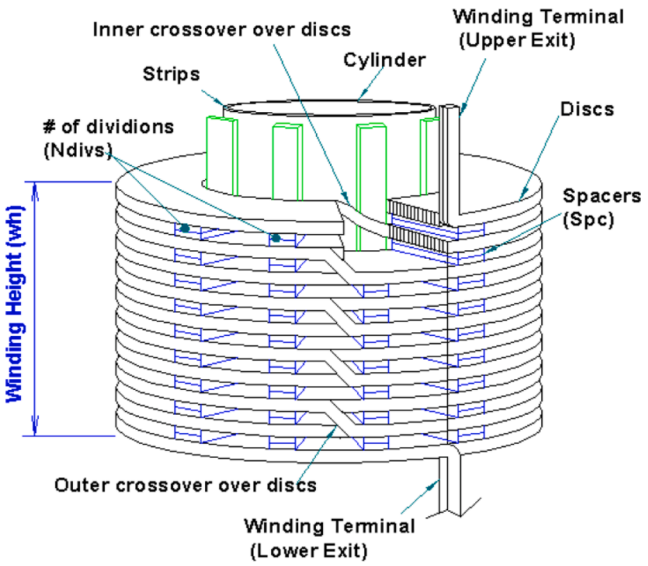

Fig. 2. Mechanical characteristics of a high-voltage winding.

A first step or initial guess, for full-scale design of power transformers and shunt reactor, is to calculate the clearances of the winding and core by using the *Weidmann design curves*, since there is no initial design data available priory. Fig. 4 describes some of the main dimensions in the winding and core [10].

Fig. 4 shows the vertical cut of a generic shunt reactor, in which some of the main geometric characteristics are: core diameter, duct or clearance between winding and core (*Bwc*), core height (*ch*), core gap height (*hgap*), winding to core surface axial clearance (*Dcs*) and limb at outer domain (*Dsl*).

In practice, power reactors have several small gaps in order to control the magnetic flux and additional winding losses as well. In the modeling perspective, since the core does not represent the investigation object, it is more effective to vary the magnetic permeability to determine the impedance values at low frequency. Usually, real power reactors have an electrostatic shield around sharp edges of the magnetic core. In this sense, the core surface can be represented as a grounded cylinder, with no influence of such small gaps, by assuming a uniform distribution of the electromagnetic parameters along the winding.

The mechanical and geometric characteristics, described in the Figs. 1–4, are fitting by an iterative procedure, which determines the electrical parameters of the shunt reactor, such as: inductance, rated voltage, nominal power, insulation coordination, frequency etc. In sequence, the test and service voltages, for line and neutral connections, are evaluated in order to define the electric insulation limits of the core and winding height.

The initial tests are carried out on a 28-MVAr single-phase reactor,

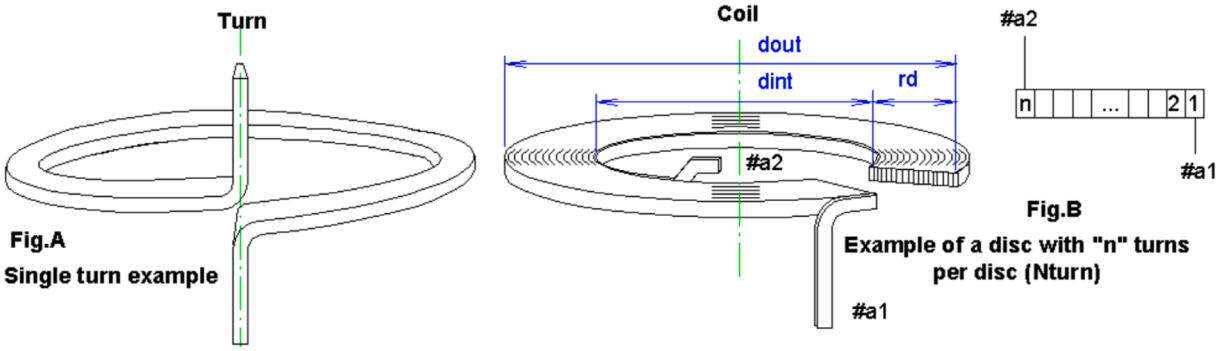

Fig. 1. Mechanical characteristics: Turns and discs structure.

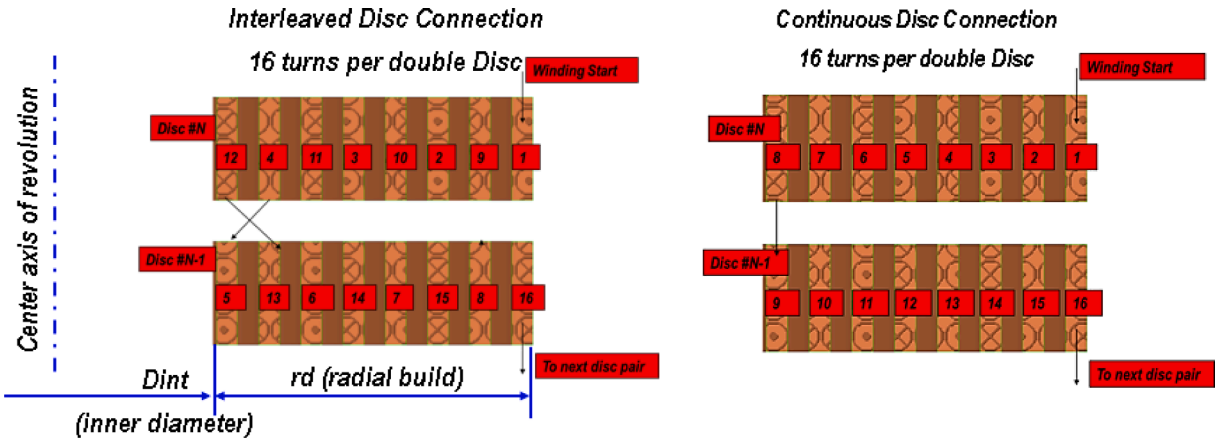

Fig. 3. Structure and connections of the DI and DO.

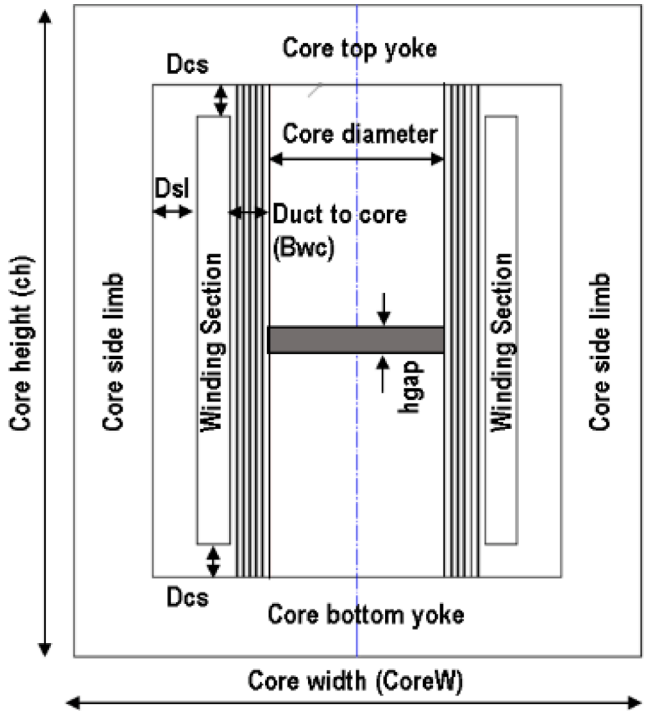

Fig. 4. Shunt reactor: front view of the winding and core.

which is connected to a 500-kV system at 60 Hz (Y three-phase with neutral to ground). The lightning (LI) and switching impulse (SI) tests must comply with 1550 and 1300 kV, respectively, and $500/\sqrt{3}$ kV phase-to-ground voltage under service. The neutral terminal must to withstand 110 kV during lightning impulse and 34 kV per one minute at industrial frequency (AV) [12,13]. The LI, SI and AV have different time scales, therefore a time conversion shows to be a proper solution to define the voltage level for the shunt reactor dimensioning. Usually, each manufacturer has its own technology to time convert and specific design curves for each voltage profile. In this sense, this research uses a common time conversion based on real applications [14,15].

The design voltage levels are calculated from the direct product of the test level to the test factor. Table 1 shows the test levels, factors and design level for each condition [13–15].

The highest voltage to the ground is 620 kV at the HV entry and 440 kV on the winding ends, such described in the Table 1. Since the voltage levels are defined, clearances and dimensioning of the reactor can be properly calculated by using a FEM-based CAD platform, as illustrated in

Table 1
Voltage Summary.

Condition	Voltage [kV]	Time Factor	Design Voltage [kV]
LI in HV entry	1550	2.5	620
SI in HV entry	1300	2.1	619
Service $500/\sqrt{3}$	318	0.67	475
LI in neutral	110	2.5	44
AC1min. in neutral	34	1.0	34

the front view of the core in the Fig. 5.

An initial guess for the cross section of the core can be calculated from an empiric formula in (1). However, such value represents an approximated diameter, since the exact one is calculate by the iterative FEM algorithm based on simulations of the magnetic flux in the core [15].

$$d_{core} = -0.00001P_{MVAr}{}^{4} + 0.0038P_{MVAr}{}^{3} - 0.3545P_{MVAr}{}^{2} + 17.11P_{MVAr}{}^{0} + 248.5 \quad (1)$$

Terms d_{core} is the initial core diameter in millimeters and P_{MVAr} is the reactor power in MVAr.

The minimum winding height can be limited to admissible creep

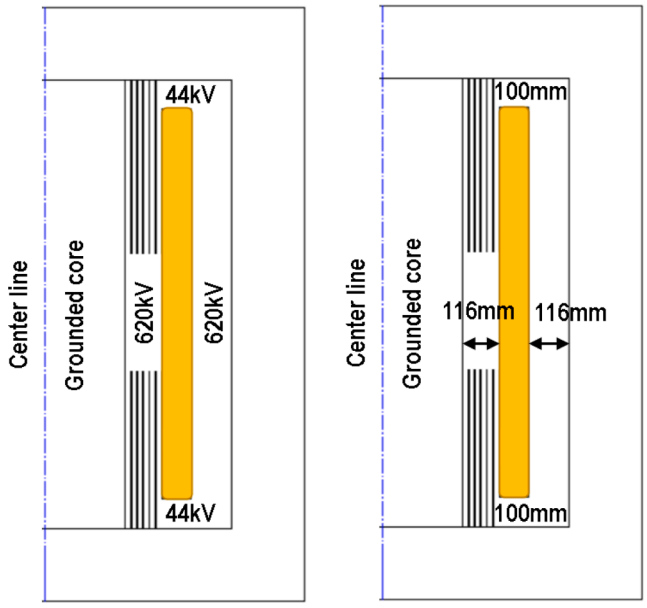

Fig. 5. Front view of the core: voltage level and dimensioning.

stress from HV entry to ground, using the *Weidmann curves* for creepage, therefore a height *wp* (Fig. 2) can be determined in (2) [15].

$$wh = 2e^{\frac{\ln(U_{DIM}/16.6)}{0.54}} \quad (2)$$

Terms U_{DIM} and *wh* are the voltage to ground for creepage and the minimum winding height in millimeters.

The core height *ch* can be limited to 3000 mm, whereas the core width is no more than 2000 mm. Such values are into the average dimension for shunt reactors, in the scale of MVAr [10,15].

The initial clearances from the core and winding to side limb can be estimated by the Weidmann curves, considering an average electric field stress of 5.3 $kV.mm^{-1}$, approximately. Thus, from the parameters *Dsl* and *Bwc* (Fig. 4), and design voltage in Table 1, we have 116.98 mm. The clearances to core yoke (*Dcs*) follow the same criteria, although the mechanical distances of the winding and core are major than requested for dielectric issues, in order to avoid eventual overheating of metallic parts and hotspots due to the leakage magnetic flux [16]. In practical terms, the shunt reactor is designed with clearance *Dcs* from 100 up to 150 mm, which does not incur in significant variations during the FEM modeling and VFT simulations, since this part is distant of the HV entry.

3. Winding structure and design

The winding represents the active part in the shunt reactor, which requires additional information for accurate FEM-based modeling, since only general characteristics and boundary conditions have been introduced so far.

$$N_{ESP} = \frac{\sqrt{2}U_{OP}}{2\pi f\, B_{core}\, S_{mag}} \quad (3)$$

Where terms N_{ESP}, U_{OP} and *f* are the total turns in the winding, rated voltage to the ground and frequency of the fundamental electric signal, respectively. The magnetic quantities B_{core} and S_{mag} are the core flux density at the center limb [*T*] and the magnetic area with proper filling factor [m^2]. This second quantity takes into account the losses on the geometric area, which is approximately 10 % in the proposed shunt reactor. The flux density is determined through a cross section of the core in which the magnetic flux seems to be linear, even under rated voltage. Thus, a linear limit of 1.65 *T* is determined for B_{core}, without affect other relevant parameters in the shunt reactor modeling for VFT simulations.

The concatenated and leakage magnetic fluxes are intrinsic related to the reactor inductance. Both quantities should converge to the total magnetic flux B_{core} in the equation (3), which represents a crucial magnetic parameter to be adjusted by the iterative FEM-based algorithm. The gap height in the core is also a crucial feature to balance the current and magnetic flux, in order to determine the inductance of the designed reactor. Thereafter the convergence of the iterative process, the total turns N_{ESP} of the winding can be defined from the following approach [17]:

$$L_{reactor} = \frac{N_{ESP}\, B_{core}\, S_{mag}}{I_{rated}} \cong \frac{N_{ESP}{}^2\, \mu_0\, S_{gap}}{h_{gap}} \quad (4)$$

Where $L_{reactor}$, S_{gap}, h_{gap} and I_{rated} are the reactor inductance [*H*], gap surface in the core [m^2], gap length [*m*] and rated current of the reactor [*A*]. The constant μ_0 is the magnetic permeability in the vacuum [$H.m^{-1}$].

The effect of spreading flux in the gap should be properly taken into account, in order to calculate B_{core} and therefore $L_{reactor}$. In this sense, a 2D axisymmetric solver for FEM modeling shows to be more efficient and accurate than some analytic formulations available in the technical literature [17,18].

Usually, in power shunt reactors from 20 up to 50 MVAr, the total winding turns should be around 3000–4000. The proposed shunt reactor is designed with 3080 turns in discs. Fig. 6 shows the main characteristics of the winding and disc configuration.

The conductor should be calculated to limit the current density with no more than 4 $A.mm^{-2}$, and the axial spacer height should be approximately 4 mm, in order to make the oil flows between discs without resistance for efficient thermal and electric insulation performances. However, the spacer height can be set with more than 4 mm, which depends of the application and electrical requirements, such as transformers and shunt reactors in GIS during VFT occurrences. The number of turns can be adjusted radially between 20 and 50 turns, whereas the number of axial discs up to 200. In the proposed 500-kV reactor, 176 discs are considered, in which 88 are connected in two axial split halves in parallel.

There are several technical literature on paper and oil insulation in power transformers and reactor. Usually, in real applications and design, the paper thickness of high-voltage windings is from 0.8 up to 2.2 mm turns. A general description of the paper thickness, as a function of the voltage level, is also established in the literature, in which 0.8–1.2 mm is recommended to impulse levels up to 1050 kV, and from 1.5 up to 2.2 mm for impulse levels up to 1550 kV [11–18]. In this article, a more careful analysis of the solid insulation is required, since the design and manufacturing of new shunt reactors, specifically for GIS applications and under VFTO occurrences, represent a relatively new and nonconventional challenge.

Finally, Fig. 7 summarizes the mechanical and geometric structure of the designed winding, in which some of the main characteristics are highlighted.

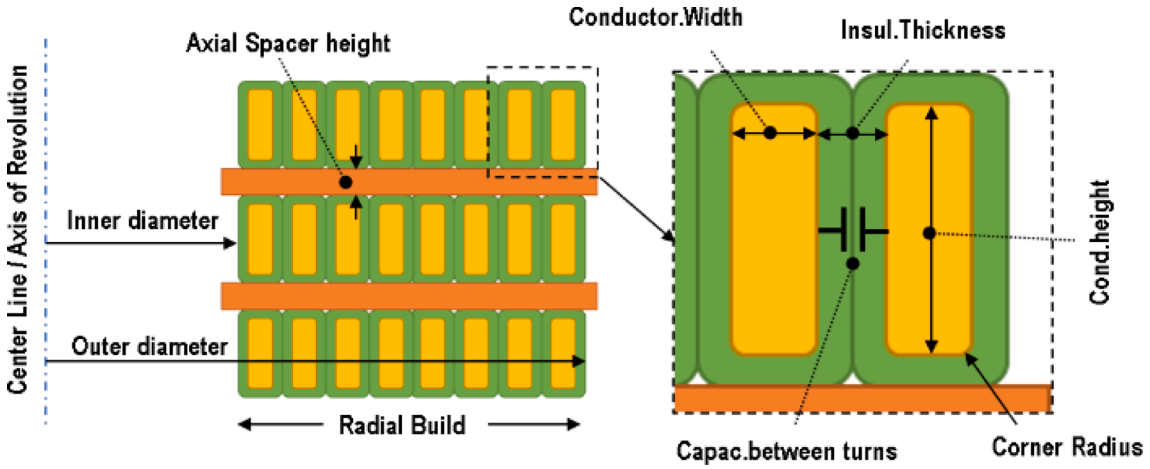

Fig. 6. Parameters of the winding with discs.

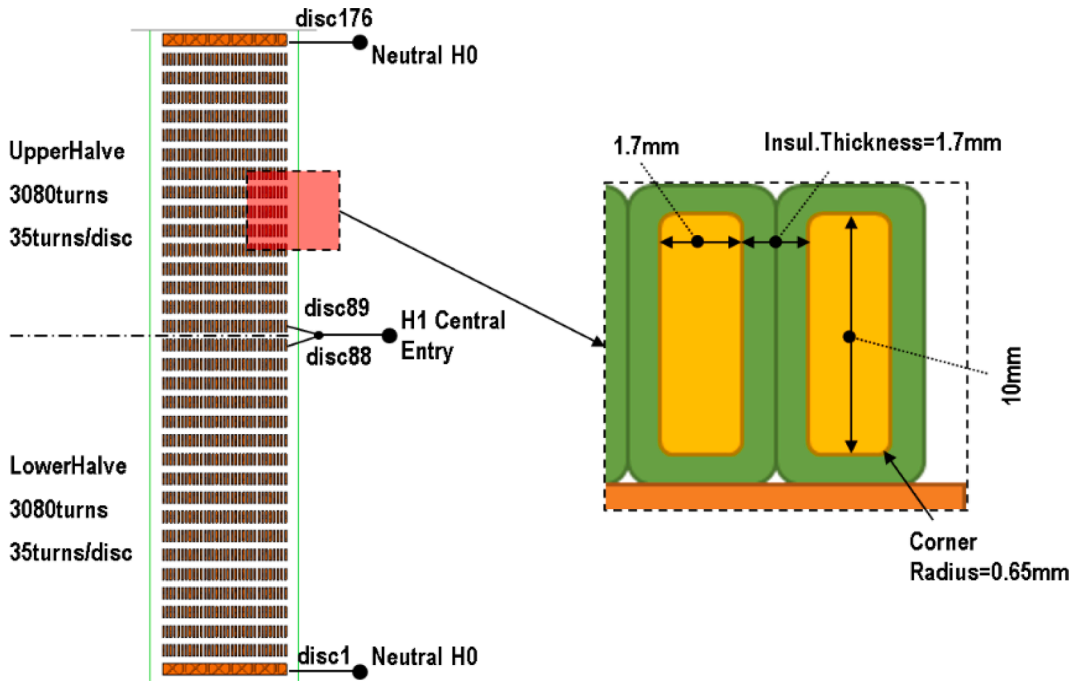

Fig. 7. Designed winding summary.

Fig. 7 shows the HV terminals (*H1 Central Entry*) and neutral terminals at the extremities of the winding (*Neutral H0*). The HV entry is located at the middle of the winding column, between discs 88 and 89, while the neutral terminals are connected to discs 1 and 176. The HV entry is at the winding middle height due to dielectric issues: sufficient creepage distance from the ground electric; and less dielectric clearances from the winding to the core, since the neutral point neutral terminals are located at the ends.

In addition, Fig. 7 describes the paper insulation with thickness of 1.7 mm between conductors in the same discs, which represents a dielectric insulation to support impulse levels up to 1550 kV [12,18].

The reactor winding was designed and manufactured following well-established standards and practical settings employed by a world-renowned manufacturer of large power transformers and shunt reactors. This same winding is evaluated in a Multiphysics CAD environment, by modeling and simulations with FEM, and thereafter validated

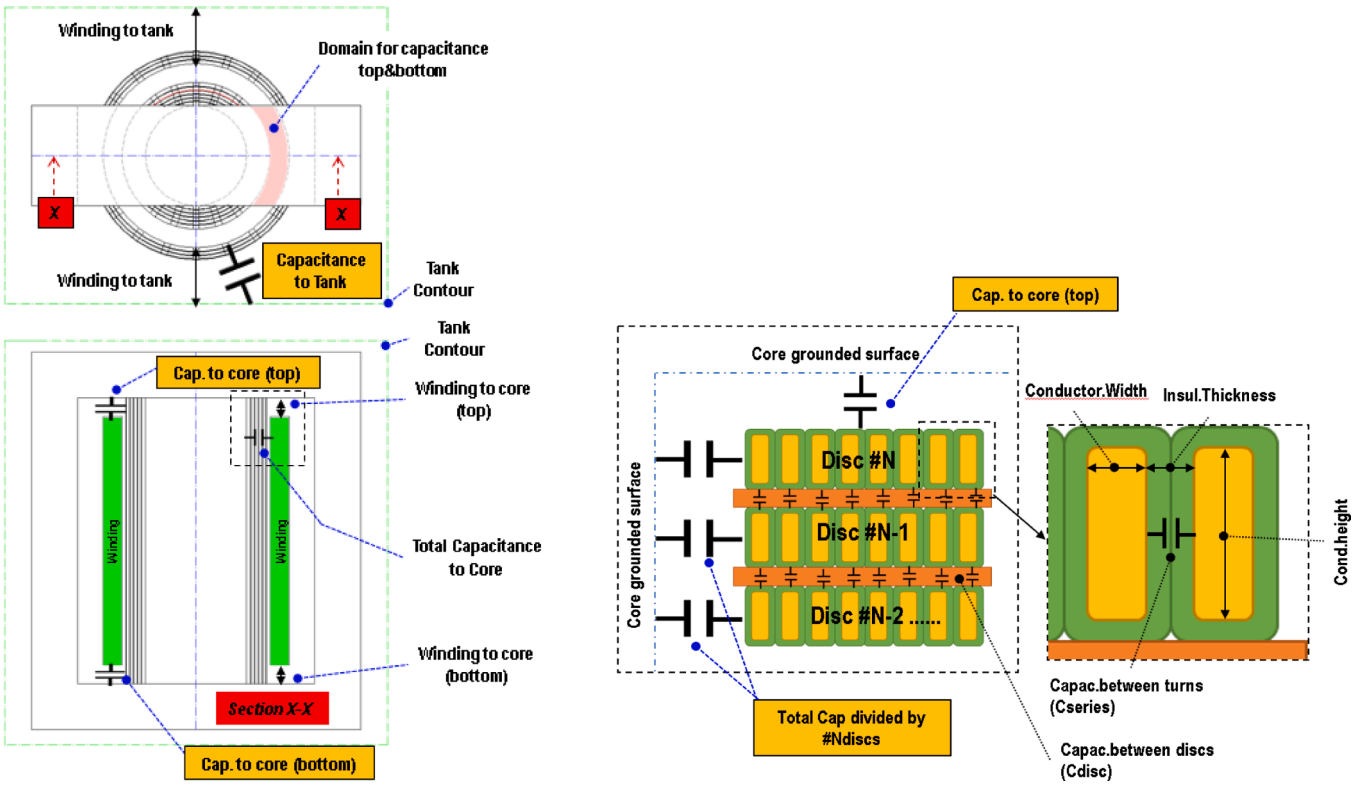

Fig. 8. Series and parallel capacitances in the winding.

from experimental results in laboratory.

4. Modeling and simulations using FEM

Since all mechanical and geometric features are prior defined, the capacitance and inductance values can be calculated and pre-processed by a FEM solver (*Siemens Magnet Simcenter*). Fig. 8 shows the main capacitance values in the winding: series capacitance (C_{series}); turn-to-turn capacitance between discs (C_{disc}); parallel capacitance to the core at inner and out diameters, to core yoke and winding to the tank.

The capacitance C_{series} can be calculated analytically, with plane capacitor formulation, or by using the FEM-based solution. However, the corner radius and field line spreading should be taken into account in the analytic formulation. Analogously; the capacitances between discs, core, tank and ground are also described in the Fig. 8; which are calculated with a planar symmetry instead of axisymmetric. The main difference in this second case is that the number of spacers between discs needs to be properly considered, since such parts play an important role in the winding and are composed of three different materials: paper insulation, spacer between discs filled with mineral oil and pressboard. In this paper, the capacitance values are directly calculated with the FEM, based on the energy stored in the electric fields.

In this research, the capacitance to the core outer limb is different than the one towards the tank, however, both magnitudes are in the same order of magnitude due to the clearances. In practical shunt reactors, the clearance from the winding to the core and from winding to tank are in the same order of magnitude, especially because the tank is not completely rectangular, with some geometric peculiarities in order to optimize the oil volume – this brings the grounded tank surface closer to the windings. Furthermore, the outer limb is a flat surface against the round shape of the outer winding diameter, i.e. a few millimeters from the minimal distance to the core. Therefore a wide distance to such surface falls in the open-oil domain, where the capacitance value could be similar. The capacitances to the inner core limb have much more influence on the winding voltage distribution, since such values are higher because of the winding clearance is significantly reduced when compared to the distance from the winding to outside grounded parts. In this sense, a special attention must be given during calculation of the inner capacitance values and capacitances to the ground.

Fig. 9 shows the equivalent model for the series capacitance, where the geometry is detailed from the left to the right side. The FEM mesh and voltage distribution are described in shaded plot at the right side. The series capacitance is 6.14 pF between strands, which is calculated in axisymmetric coordinates based on the mean winding diameter.

The capacitance between discs can be represented as planar capacitors, which are modelled using the FEM, as described in the Fig. 10-A. If *Ndivs* and *Spacer Width* are unknown, a relationship of 27 %–35 % of pressboard to oil can be used, as in Fig. 10-B. The depth here is the radial build *Rd*.

For the capacitance between winding to the core and winding to side limb, a top viewed model can be used where the *Ndivs* and *strip width* are needed. In addition, some parameters could not be available for the winding modeling, therefore values from 15 up to 35 mm are usually found in the literature and industrial practices [15,17,18].

The previously defined dimension *Bwc* need to be subdivided into small oil ducts and cylinders, in order to limit the gradient where ducts of 10 mm are considered. The *Ndivs* represents a mechanical-thermal parameter to the winding design, which can be defined splitting the circumference into approximately 100 segments, and then determining *Ndivs*.

Thus, a cylindrical symmetry is defined for the winding height, as shown in Fig. 11, in which the same energy approach is considered for the electric field. The capacitance is 1034.11 pF with *Ndivs* = 20, strip width 25 mm and *Bwc* divided in 11 ducts with 9.63 mm width, 10 cylinders with 1 mm thickness.

The winding turns and discs are modeled in the axisymmetric mode and real scale. The core is modeled with an effective magnetic permeability without the gap. In shunt reactors, the relative permeability value is from 7.53 up to 12.14, in the proposed winding modeling arrangement.

The Fig. 12-A illustrates a real winding, while Fig. 12-B and 12-C describe a double disc with 16 turn and the equivalent electric circuit, respectively. The equivalent circuit represents the mutual capacitances between core, discs and turns. Each coil represents a real solid strand (Fig. 12-B) and the boundary condition *coil* is applied to start and finish of each turn. Fig. 12-D shows the designed winding with 35 turns/disc in full DI arrangement (total 176 discs). The core is modeled with the mechanical and geometrical characteristics priory described, with some adjustment in the relative magnetic permeability to 10.34, in order to determine the nominal inductance at fundamental frequency of the power signal.

5. Evaluation of simulations and experimental results

In this section, the time- and frequency-domain results, obtained from simulations with the FEM-based model and experimental tests, are compared and discussed. First, the frequency-dependent impedance results, obtained with computational simulations and *Sweep Frequency Response Analysis* (SFRA), are evaluated from 10 Hz up to 1 MHz. The frequency scan is carried out directly on the full-scale winding of the designed shunt reactor, in which the highest natural frequencies are determined and thereafter compared to the same values obtained with the FEM-based model.

In sequence, a time-domain analysis is presented, where the VFTs and electric fields in the shunt reactor are properly evaluated based on simulation and experimental results. This analysis is crucial to detect and locate transient overvoltages between turns and discs in the winding, with more than 3000 turns and 2.11 m high.

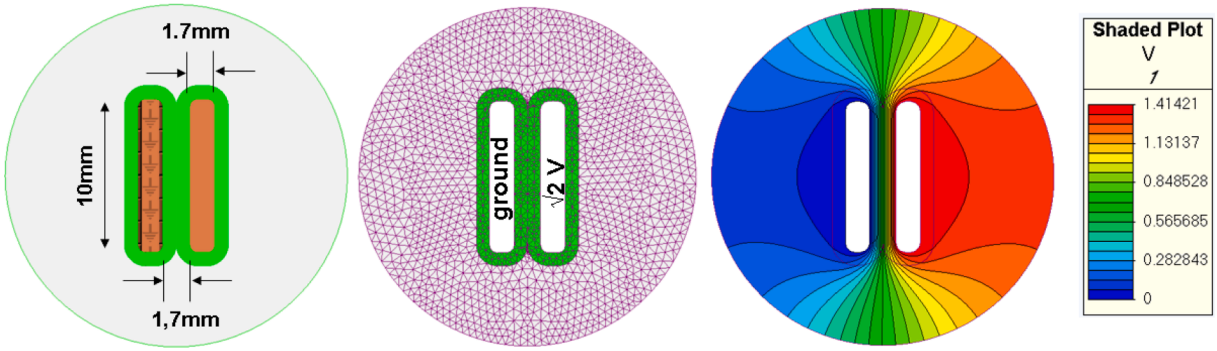

Fig. 9. Calculation of the series capacitance.

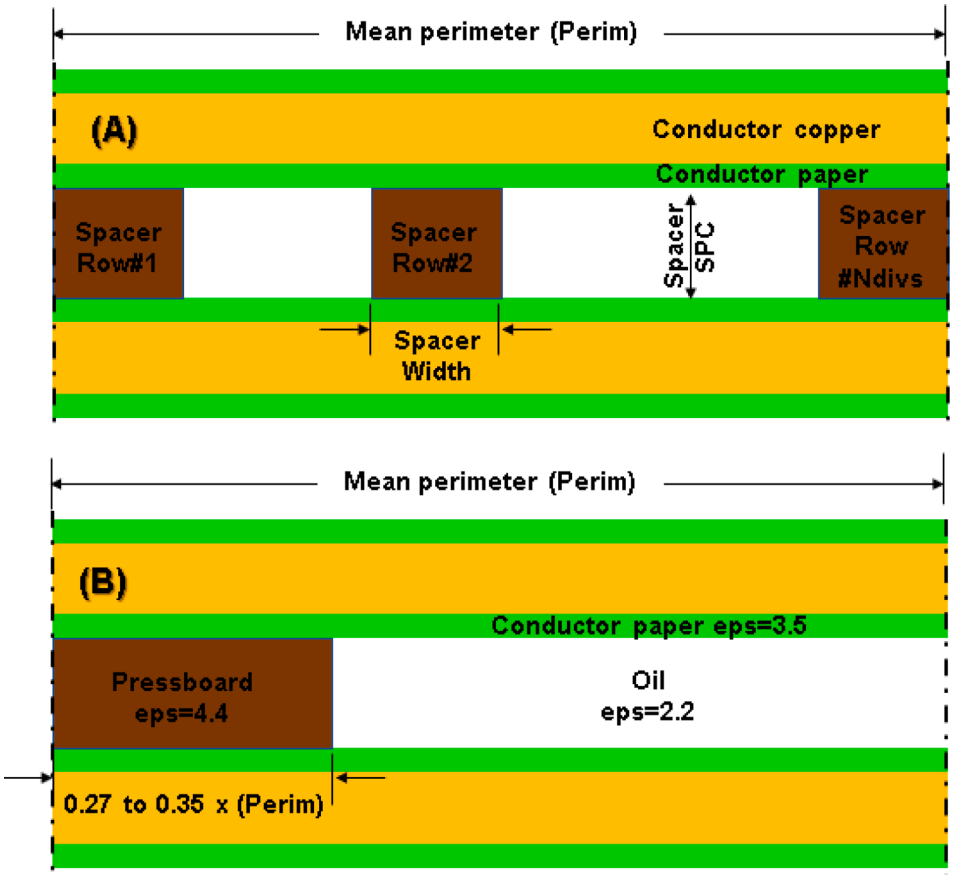

Fig. 10. Capacitance between discs.

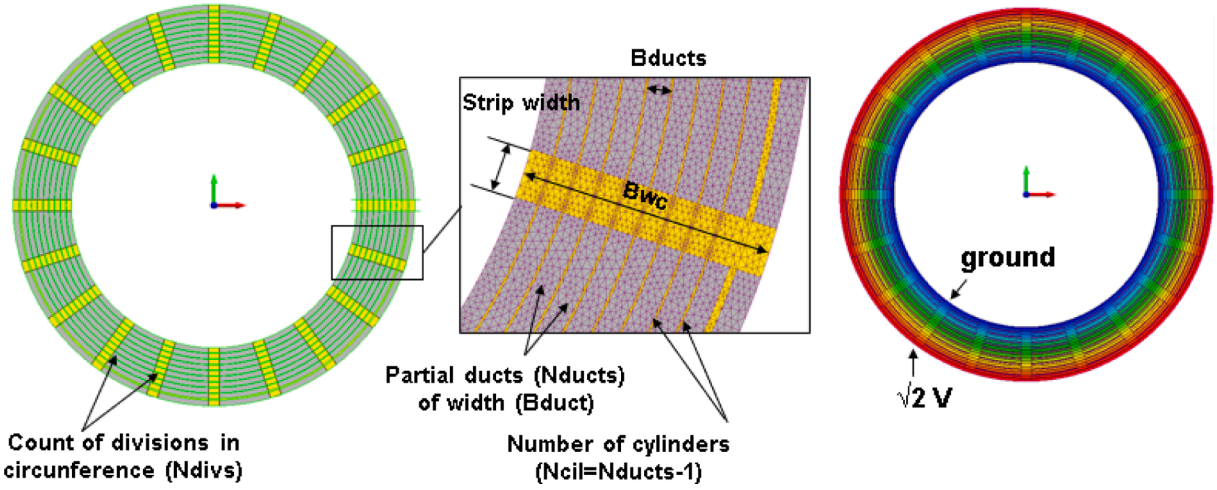

Fig. 11. Capacitance winding to core scheme.

5.1. Assessment in the frequency domain and SFRA

The winding of the 28-MVAr shunt reactor is scanned from 10 Hz to 1 MHz, with 181 frequency samples logarithmic spaced within decades. The frequency sweeping is performed with two different frequency generators: an analog generator with frequencies up to 1.02 MHz; and a digital source up to 2.05 MHz and resolution of 1 kHz. Fig. 13 describes the laboratorial structure for the SFRA.

The winding is properly grounded and submitted to a frequency-varying AC signal at the HV entry. The frequency response, with amplified and attenuation points, is monitored with a few *taps* connected directly to the turns and discs, such as described in the Fig. 13.

The frequency response of the winding, obtained via experimental data and simulations with FEM, is described in the Fig. 14.

The frequency-dependent impedance profiles, obtained from measurement and simulation, show to be approximately similar. Some variations are observed from 2 kHz up to 10 kHz, and minor differences from 10 to 200 kHz. This means that the inductive network represents properly the designed shunt reactor, mainly because of the range up to 1 kHz. In addition, the first resonance point appears near to 3 kHz in both

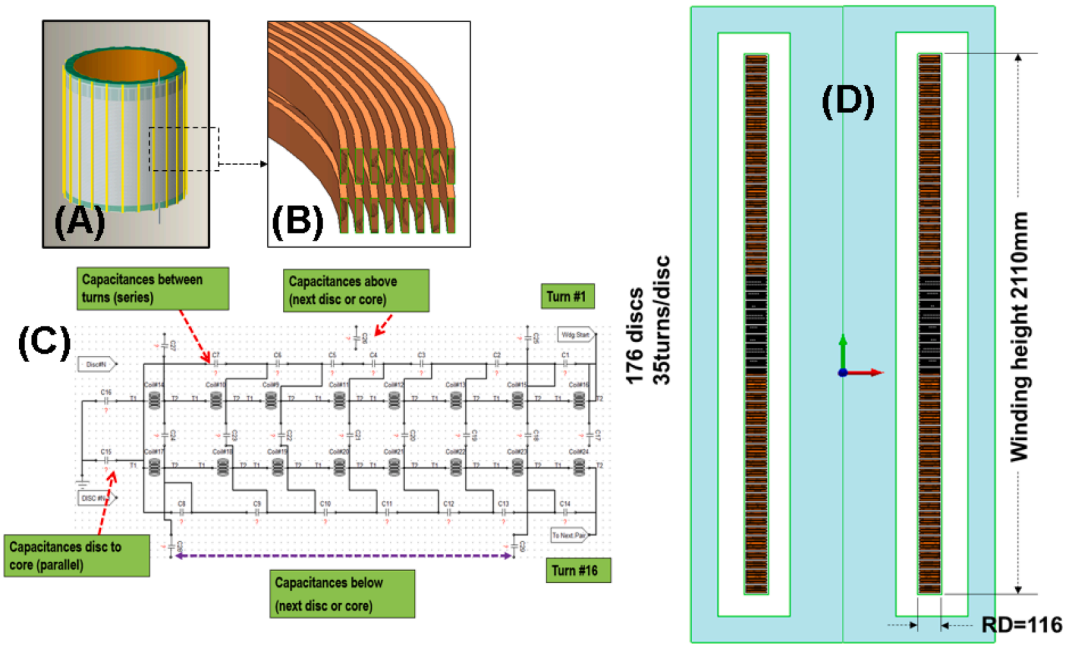

Fig. 12. DO modelled in FEM environment with capacitances connected.

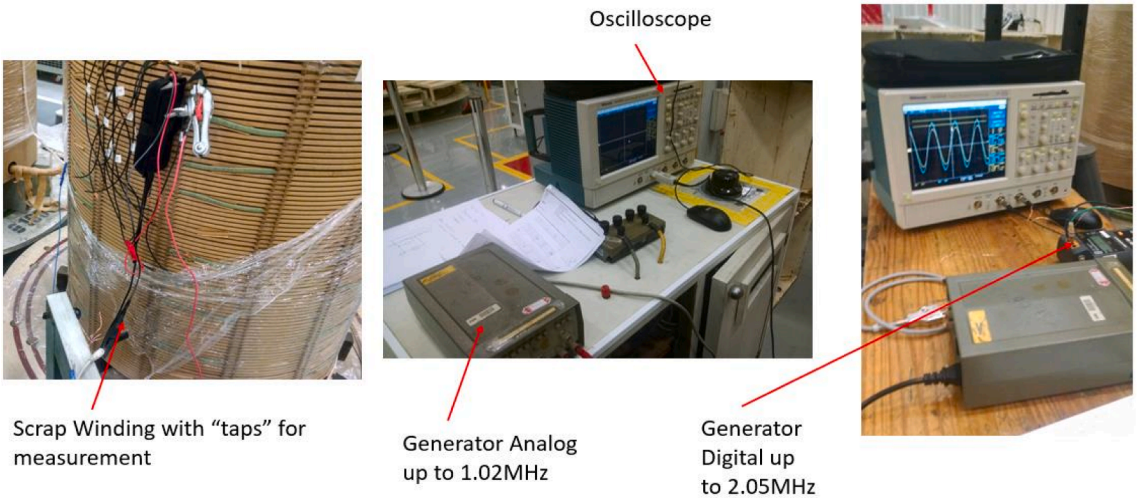

Fig. 13. Laboratorial arrangements for the SFRA.

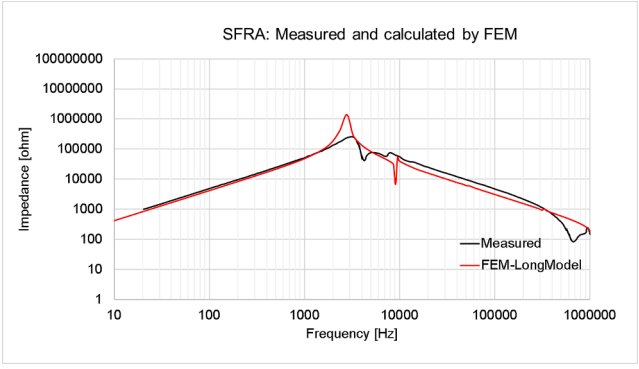

Fig. 14. SFRA: experimental data and simulations with FEM.

measured and simulated scans. The main differences between experimental data and simulations can be attributed partially to inaccuracies of the measuring apparatus, while variations from 1 kHz to 10 kHz occur because of the core modeling with a constant magnetic permeability combined to the turns per disc and overall winding design [19]. At very high frequencies, 100 kHz up to 1 MHz, small inaccuracies in the grounding representation and winding inductances can leads to significant variations in the SFRA simulations [19,20].

Table 2 shows the measured and simulated frequencies in which the natural oscillations occur from 500 kHz. Although the differences observed in the Fig. 14, the natural frequencies simulated with the FEM-based model show a great similarity with results obtained from experimental data.

5.2. Analysis of the VFTs and electromagnetic fields in the winding

A laboratorial structure was developed with a repetitive wave generator with voltage doubler, in order to reproduce the VFTs. This

Table 2
Natural frequencies obtained from the SFRA.

Measured [kHz]	Calculated [kHz]
2023	2011
1755	1692
1658	1603
1317	1450
1250	1211
1175	1196
1035	988
880	885
770	778
658	642

wave generator is composed of spherical electrodes with air gap, which are connected by a pneumatic drive. An oscilloscope with 350 MHz and high resolution (5G samples per second and probes with 100 MHz) is used for measuring a wave front with 13 ns and voltage peak of approximately 1 kV.

Fig. 15 shows the designed winding connected to the measuring apparatus (oscilloscope and taps) and wave generator.

The high-voltage surge with fast wave front results in an oscillatory voltage profile between turns and discs, especially those near to the HV entry of the winding.

Fig. 16 describes the voltage impulse applied at the HV terminal of the winding, and measurements between turns and discs. The voltage signal shows a rise time of 13 ns, with 13.4 ns from 1 kV peak to −800 V. The following graph shows the voltage measuring between conductors at the external diameter of the entry disc of the winding (near to the HV entry), which shows an oscillatory behavior with magnitude of 100 V. Finally, the voltage profile is described between the external conductors, at the outer diameter of the discs 87 and 88. The same voltage measuring is presented for discs 70 and 71, which corresponds to 20 % of the

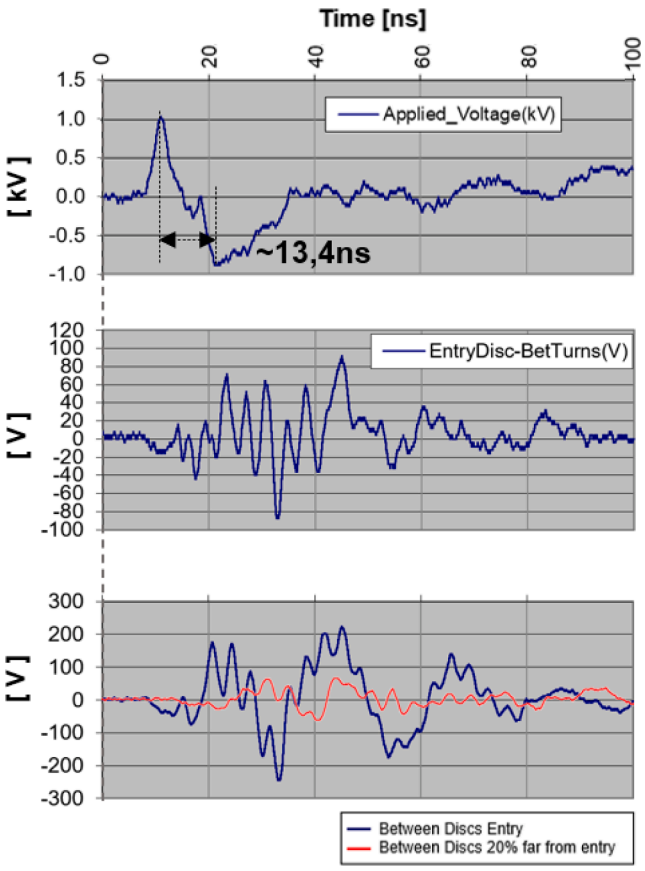

Fig. 16. Experimental tests: voltage profiles in the winding.

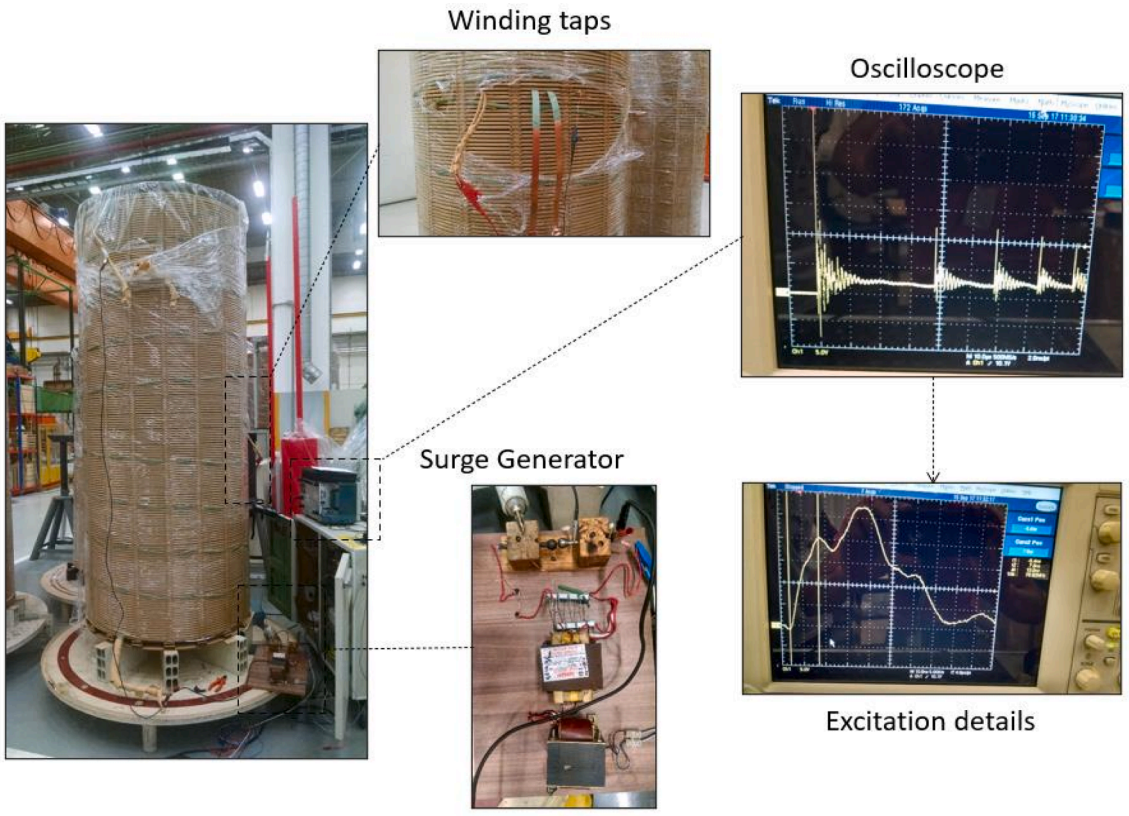

Fig. 15. Laboratory structure for VFT tests.

winding length, from the grounding connections at the ends. In this same figure, it is possible to verify the propagation time of the voltage surge from the HV entry, comparing the applied voltage wave to the surge between discs 70 and 71. The curves are in different voltage scales and throughout the same time axis.

The same procedure is carried out with the FEM-based computational model, considering a reduced time step and total simulation of 300 ns. Fig. 17 illustrates the transversal section of the designed winding, in which the measured discs are highlighted. Discs 88 and 89 are the HV entry of the winding, whereas discs 73 and 74 represent approximately 20 % from the grounding terminals of the designed shunt reactor.

Fig. 17 shows the simulated voltage impulse at the HV terminal of the winding model, which is characterized by a similar 13/150-ns wave, which is denoted as V1. The simulated voltages C766 and C1792 are between turns in the disc and between discs at the HV entry, respectively. In addition, C768 is the voltage between the first disc at the HV entry and the adjacent one, which was not measured during the experimental tests. Finally, C96 is the voltage signal between discs 73 and 74, near to the grounding terminal of the shunt reactor.

Table 3 presents a comparison of the maximum voltage obtained from measured data and simulation.

Results in the Table 3 show the simulated voltage V766 4 % minor than the same value measured during experimental tests. The voltage peaks of V1792 and V96 are 12 % and 25 % higher than the same measured values, respectively. These variations are expected, in view of the high complexity of the winding design and modeling for VFT simulations, which represents a very specific application. In addition, small variations in the design (e.g. winding structure, geometry, material and

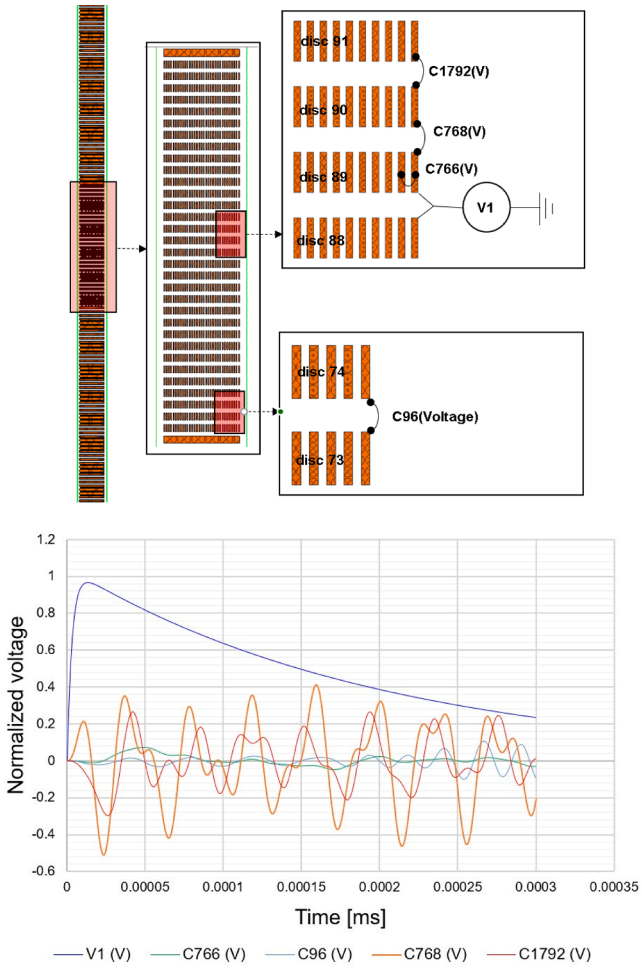

Fig. 17. Computational simulation: voltage profiles in the winding.

Table 3
Error between measured and simulated voltages.

	Measured [p.u.]	Simulated [p.u.]	Error [%]
V766	0.081	0.078	4
V768	–	0.511	–
V1792	0.245	0.295	12
V96	0.08	0.1	25

environment), experimental tests (measuring and input signal) and computational modeling could lead to significant errors between experimental and simulated results. For example, even the measuring tap connection to the winding or humidity variation of the air and paper insulation could imply in errors between measurement and simulation.

In addition, the VFTO propagation can be assessed from the dynamic behavior of the electric field distribution in the winding. The time-varying profile of the electric field can be observed with the equipotential lines across the turns and discs, which are moving from the outer diameter to the internal section of the winding structure, as shown in the Fig. 18. The voltage surge propagation through the capacitive circuit of the winding is described by each image in the Fig. 18, in time scale of nanoseconds.

Since the electric potential and field are mapped in the entire winding, the insulation between turns and discs can be properly evaluated. The electric insulation between turns is composed of paper with thickness 1.7 mm and spacers between discs are 4 mm. The FEM-based modeling simulates the maximum electric gradients on the extremities of the turns and discs, during the VFTs resulted from the 13/165 ns voltage wave applied at the HV entry of the winding. The electric field mapping between turns is described in the Fig. 19.

Based on the simulated results in the Table 3, the maximum voltage between turns is approximately 70 kV; electric gradient in the paper is 40 kVmm; maximum potential between the entry discs is 459 kV; and gradient between such discs is approximately 115 kV/mm. The maximum gradient supported in paper insulation is 90 kV/mm, which means that the full-scale reactor was properly designed [12].

6. Conclusion

The design, manufacturing and test validation of a full-scale shunt reactor, for gas insulated environment, were thoroughly described in this paper. An introduction was presented on the main parts and general structure of the winding, such as paper insulation definitions and configuration in turns and discs. In this context, a complete testing methodology was described based on the FEM-based modeling of the winding and experimental evaluation in laboratory.

The proposed CAD model represents accurately the capacitive effects in the winding, which are demonstrated by the VFT simulations and resulting electric fields between turns and discs. Such results are validated based on the same results obtained from experimental tests with the designed shunt reactor. The simulated frequency- and time-domain results show great adherence to experimental data in laboratory (SFRA and VFTO simulations). Nevertheless, the model reliability depends on the prior knowledge of the electric parameters, which can be accurately obtained by using the proposed FEM-based modeling technique.

Since the electric gradients are properly determined by using the FEM, important features of the shunt reactor can be predefined, which leads to an optimized design and manufacturing of the full-scale winding for experimental tests.

The FEM-based solution and modeling techniques are combined to determine the VFT assessment methodology; i.e. the original contribution of the manuscript is the systematic process applied to produce a real power reactor for GISs (conception, design, manufacturing, computational and experimental tests), which represents a theoretical and practical contribution for both academic and industrial society. In this

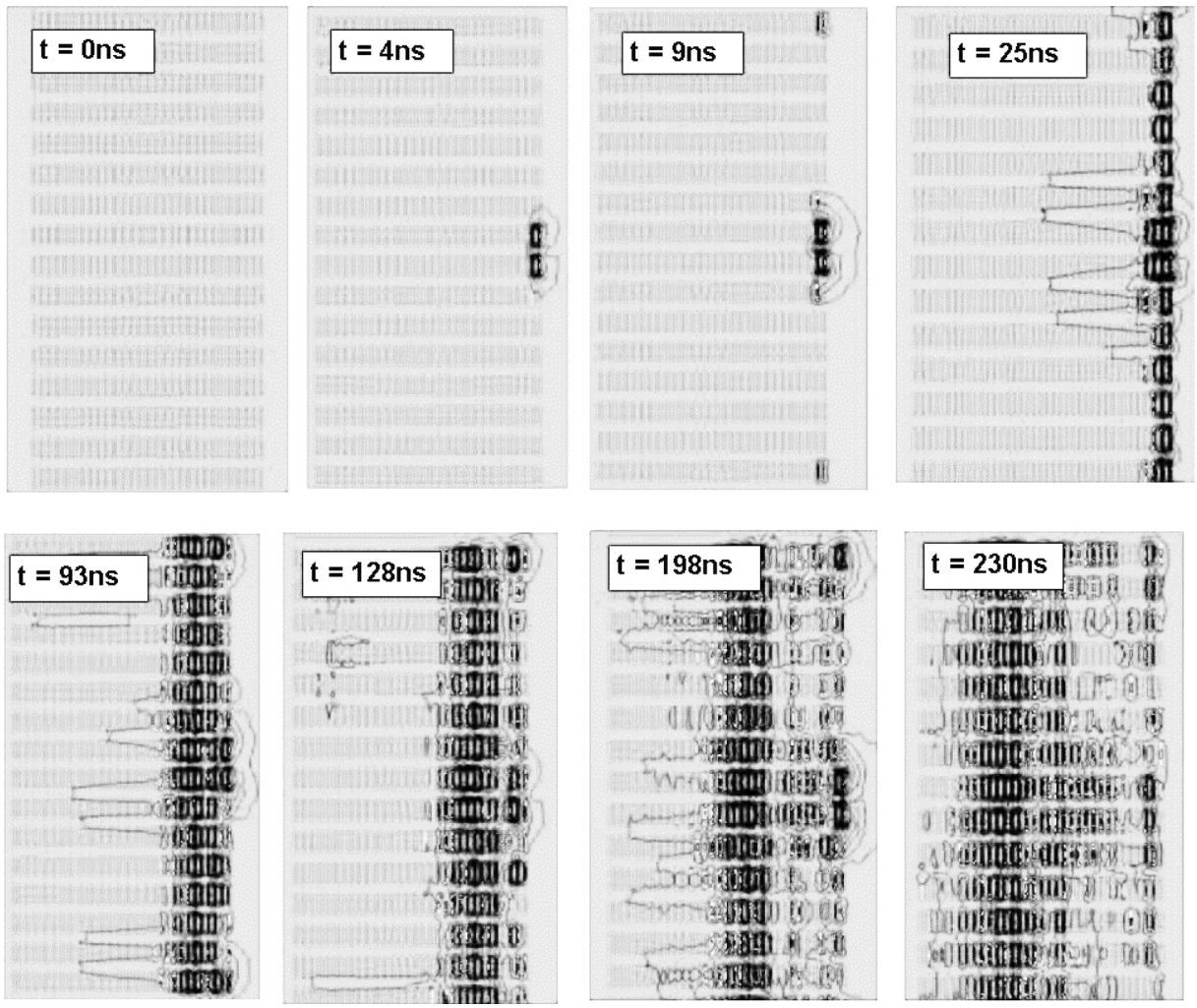

Fig. 18. Electric potential distribution through the winding.

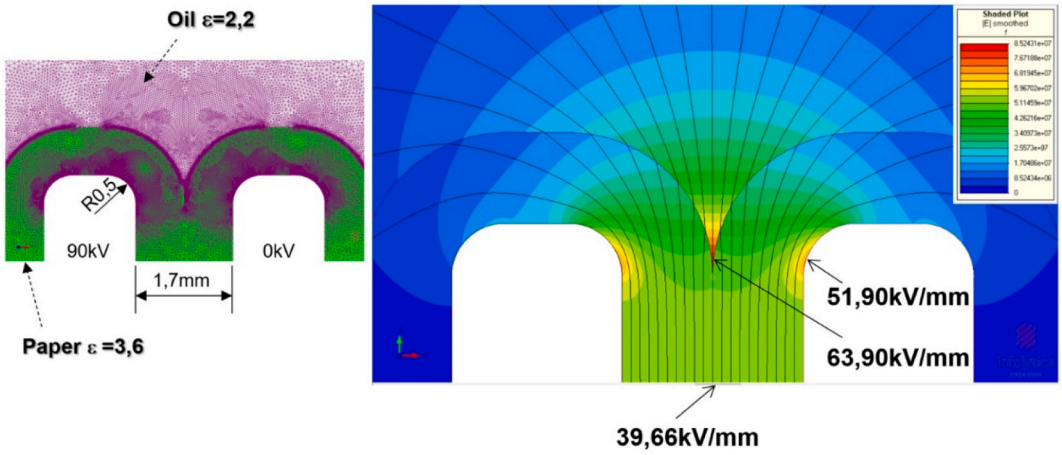

Fig. 19. Electric gradient mapping between turns.

sense, our manuscript aims to determine a guideline for design and manufacturing of power reactors for gas insulated environment, more specifically for VFT analysis.

Declaration of competing interest

The authors declare that they have no known competing financial interests or personal relationships that could have appeared to influence the work reported in this paper.

Data availability

Data will be made available on request.

References

[1] Moreau O, Dos Santos G, Guillot Y. Computation of very fast transient overvoltages inside transformers resulting from switchings. In: International conference on power systems transients (IPST'05), Montreal, Canada; 2005.

[2] Riechert U. Very fast transients overvoltages (VFTO) in gas *insulated* EHV & UHV substations. In: IEEE PES Switchgear Committee, 2012 Fall Meeting, San Diego, USA; 2012.

[3] Hashemnia N, Abu-Siada A, Masoum MAS, Islam SM. Characterization of transformer FRA signature under various winding faults. In: IEEE international conference on condition monitoring and diagnosis, Bali, Indonesia, 2012. p. 446–9.

[4] Caballero PT, Costa ECM, Kurokawa S. Frequency-dependent line model in the time domain for simulation of fast and impulsive transients. Int J Electr Power Energy Syst 2016;80:179–89.

[5] Nagarsheth R, Singh S. Study of gas insulated substation and its comparison with air insulated substation. Int J Electr Power Energy Syst 2014;55:481–5.

[6] Elkins DI, Jain AC, McDermott TE, Rees V. Transients during 138-kV SF6 breaker switching of low inductive currents. IEEE Trans Ind Appl 1993;29(4):721–7.

[7] Alexandru M, Czumbil L, Polycarpou A, Nouri N, Andolfato R, Micu DD. Mitigation of transient ground potential rise in gas insulated substations during very fast transient overvoltage. Electr Pow Syst Res 2022;207:107824.

[8] Georgilakis P. Spotlight on modern transformer design. 1st ed. Greece: Springer Press; 2009.

[9] Pedersen K, Lunow ME, Holboell J, Henriksen M. Detailed high frequency models of various winding types in power transformers. International conference on power systems transients (IPST'05), Montreal, Canada; 2005.

[10] Rahimpour E, Tenbohlen S. Experimental and theoretical investigation of disc space variation in real high-voltage windings using transfer function method. IET Electr Power Appl 2010;4:451–61.

[11] Thomas B, Savadamuthu U. Impulse breakdown characteristics of aged oil impregnated paper. IEEE Trans Dielectrics Electrical Insul 2017;24(4).

[12] IEC 60076-3 Insulation levels, dielectric tests and external clearances in air; 2018.

[13] IEC 60076-1 power transformers – general; 2011.

[14] IEEE Std C57.12.10-2017 standard requirements for liquid-immersed power transformers; 2017.

[15] Karlsen R, Løvlien S, Parma D. Transformer handbook. Switzerland: Business Unit Transformers ABB; 2004.

[16] Melo AS, Calil WV, Costa ECM, Liboni LHB, Di Santo SG. Identifying hot spots in GSU power transformers using multiple methods. IET Sci Measur Technol 2020;14 (2):233–40.

[17] Karsaid K, Kerényi D, Kiss L. Large power transformers. Elsevier; 1987.

[18] Ziomek W, Kuby D, Franchek M. High voltage power transformer insulation design. In: The IEEE electrical insulation conference, Annapolis, Maryland, USA; 2011.

[19] Wu L, Wouters H, Steennis E. Influence by parasitic capacitances on frequency response of a 380–150–50 kV transformer with shunt reactor. In: The 18th international symposium on high voltage engineering – ISH, Seoul, Korea; 2013.

[20] Ibrahim K, Korany N, Saleh S. Effects of power transformer high frequency equivalent circuit parameters non-uniformity on fault diagnosis using SFRA test. Ain Shams Eng J 2022;13(4):101674.